# REPORT DOCUMENTATION PAGE

Form Approved OMB NO. 0704-0188



| 1. REPORT DATE (DD-MM-YYYY) | 2. REPORT TYPE | 3. DATES COVERED (From - To) |
|---|---|---|
| 06-05-2021 | Final Report | 12-May-2014 - 11-Nov-2020 |

**4. TITLE AND SUBTITLE**
Final Report: Non-equilibrium Dynamics with Ultracold Atoms

**5a. CONTRACT NUMBER**
W911NF-14-1-0154

**5b. GRANT NUMBER**

**5c. PROGRAM ELEMENT NUMBER**
611103

**6. AUTHORS**

**5d. PROJECT NUMBER**

**5e. TASK NUMBER**

**5f. WORK UNIT NUMBER**

**7. PERFORMING ORGANIZATION NAMES AND ADDRESSES**
University of California - Santa Barbara
3227 Cheadle Hall
3rd floor, MC 2050
Santa Barbara, CA 93106 -2050

**8. PERFORMING ORGANIZATION REPORT NUMBER**

**9. SPONSORING/MONITORING AGENCY NAME(S) AND ADDRESS (ES)**
U.S. Army Research Office
P.O. Box 12211
Research Triangle Park, NC 27709-2211

**10. SPONSOR/MONITOR'S ACRONYM(S)**
ARO

**11. SPONSOR/MONITOR'S REPORT NUMBER(S)**
62132-PH-PCS.14

**12. DISTRIBUTION AVAILIBILITY STATEMENT**
Approved for public release; distribution is unlimited.

**13. SUPPLEMENTARY NOTES**
The views, opinions and/or findings contained in this report are those of the author(s) and should not contrued as an official Department of the Army position, policy or decision, unless so designated by other documentation.

**14. ABSTRACT**

**15. SUBJECT TERMS**

| 16. SECURITY CLASSIFICATION OF: | | | 17. LIMITATION OF ABSTRACT | 15. NUMBER OF PAGES | 19a. NAME OF RESPONSIBLE PERSON |
|---|---|---|---|---|---|
| a. REPORT | b. ABSTRACT | c. THIS PAGE | | | David Weld |
| UU | UU | UU | UU | | 19b. TELEPHONE NUMBER 805-893-7634 |

# RPPR Final Report
as of 07-May-2021

Agency Code: 21XD

Proposal Number: 62132PHPCS **Agreement Number: W911NF-14-1-0154**
**INVESTIGATOR(S):**

**Name:** David M. Weld
**Email:** weld@physics.ucsb.edu
**Phone Number:** 8058937634
**Principal:** Y

Organization: **University of California - Santa Barbara**
Address: 3227 Cheadle Hall, Santa Barbara, CA 931062050
Country: USA
DUNS Number: 094878394 EIN: 956006145W
**Report Date:** 11-Feb-2021 Date Received: 06-May-2021
**Final Report** for Period Beginning 12-May-2014 and Ending 11-Nov-2020
**Title:** Non-equilibrium Dynamics with Ultracold Atoms
**Begin Performance Period:** 12-May-2014 **End Performance Period:** 11-Nov-2020
**Report Term:** 0-Other
Submitted By: David Weld Email: weld@physics.ucsb.edu
Phone: (805) 893-7634


**STEM Degrees:** 6 **STEM Participants:** 10

**Major Goals:** Understanding the time evolution of strongly interacting quantum systems is central to many outstanding challenges in physics, on scales ranging from the crystalline to the cosmological. Major advances in our knowledge and control of non-equilibrium many-body quantum dynamics would have fundamental importance for quantum statistical physics, and could have applications to phenomena across a broad range of energy scales, from heavy ion collisions and early-universe physics to spintronics, material growth, and quantum information processing. Additionally, improved knowledge and control of coherent many-body quantum evolution will be required for the scaling of any quantum computing architecture to large numbers of qubits. Existing theoretical tools for addressing non-equilibrium quantum phenomena in large systems are few and limited, which heightens the importance of experimental input. However, controllable and well-defined tests of non-equilibrium dynamics have been difficult to implement in condensed matter systems, because of rapid relaxation times and non-variable system parameters like tunneling rate or interaction strength. In contrast, the convenient relaxation timescales and exquisite controllability of cold atomic systems makes them a nearly ideal context in which to experimentally address questions of non-equilibrium quantum dynamics. Such questions have attracted interest since the early days of ultracold atomic physics experiments. Optical lattices in particular have opened new opportunities for non-equilibrium studies of topics like quench dynamics in the superfluid–Mott insulator phase transition, the subtle interplay between integrability and ergodicity in one-dimensional Bose gases, and many-body Landau-Zener dynamics. However, the tunneling timescales of the most commonly trapped heavy atomic species (sodium and rubidium) are very slow, especially when compared to finite heating rates. This problem, along with limitations on real-time control and shaping of lattice potentials, has restricted the development of experimental cold-atom non-equilibrium dynamics. Now, the field of cold atom non-equilibrium dynamics is ripe for a transition from measurement to quantum control of many-body states and Hamiltonians. Unlike ionic lattices, optical lattices can be fully controlled in both space and time. This control of the potential, along with Feshbach-enabled control of the interaction strength, makes it possible to study the consequences of extending the translation-symmetry-breaking of the lattice into the time domain, and to exert full quantum control over Hamiltonian parameters varying in both space and time. In our ARO-sponsored work, we proposed to build a new experimental platform to enable a broad range of fundamental experiments in controlled non-equilibrium many-body quantum dynamics. This fast, flexible quantum simulator was to use low-mass, fast-tunneling ultracold lithium atoms in dynamically reconfigurable optical potentials to experimentally investigate two broad classes of non-equilibrium phenomena: quantum quenches and driven systems. In a quantum quench, a sudden change in a parameter of the

Hamiltonian is used to prepare a highly non-equilibrium state, the resulting dynamics of which can be studied as a function of time. Fundamental unanswered questions which we proposed to address include the nature of thermalization or equilibration after a quench, the study of excitations produced by nearly adiabatic ramps through quantum phase transitions, and the effect on post-quench dynamics of dimensionality, finite temperature, and density inhomogeneities. Driven systems, by contrast, are described by Hamiltonians with periodically time-varying parameters. Many important many-body phases (e.g. quantum Hall states) depend for their existence on time-reversal symmetry breaking. On an even more basic level, the conservation of energy itself depends on continuous time-translation symmetry. In a condensed matter context, time-reversal symmetry breaking is generally achieved using a magnetic field, and experiments which break continuous time-translation symmetry using ultrafast lasers are a current frontier of research. Cold atomic systems offer the opportunity to directly break time-reversal and time-translation symmetry at ultrafast-equivalent timescales using driving terms in the Hamiltonian, opening up a broad class of experiments which would be difficult or impossible in electronic solids. Applications of driven systems which we plan to investigate include dynamic localization in Kapitza optical lattices, quantum chaos, and preparation of topologically nontrivial states. We proposed to first build an apparatus enabling investigations of non-equilibrium phenomena, then to embark upon six related research projects with the overarching objective of achieving breakthroughs in our understanding and control of strongly interacting quantum systems far from equilibrium. The proposed program of research thus has seven ambitious main goals: Goal 1: (Year 1) Develop cold lithium apparatus with dynamically configurable optical traps. Goal 2: (Year 2) Demonstrate dynamic stabilization in a modulated lattice. Goal 3: (Year 3) Measure the effects of interaction on quantum chaotic behavior. Goal 4: (Year 3) Measure quench dynamics in single-component and two-component systems. Goal 5: (Year 4) Experimentally test eigenstate thermalization hypothesis. Goal 6: (Year 4) Develop techniques for the preparation of topologically nontrivial states. Goal 7: (Year 5) Detect topologically nontrivial states in cold-atom samples.

**Accomplishments:** Accomplishments for this reporting period are described and illustrated in the attached pdf.

**Training Opportunities:** This project has provided continuous opportunities for training and professional development of both graduate and undergraduate students at UCSB. Graduate students Ruwan Senaratne, Zach Geiger, Kevin Singh, MIsha Lipatov, Cora Fujiwara, Quinn Simmons, Roshan Sajjad, and Jeremy Tanlimco have all developed their technical and scientific skills as part of our work towards the goals of the project. Cora, Zach, Kevin, and Ruwan received PhDs during the grant period. In addition to intensive training in the experimental techniques of quantum optics and the production of quantum degenerate gases, which takes up the majority of a graduate student's time in this field, graduate students involved with the project have also built their skill sets in particular specialized areas, such as topological transport dynamics, theories of quantum chaos, and RF electronics. Regular attendance and public presentations at conferences (including virtual ones in the COVID era) has been a key professional development activity for all participating graduate students. Many UCSB undergraduates, including Alec Cao, Max Prichard, and Jack Pan, have also benefited from training opportunities associated with the goals of this proposal. Alec and Max were both awarded Goldwater Scholarships in 2020, and Alec is a 2021 Churchill fellow.

**Results Dissemination:** Dissemination of the results of the project was achieved via journal publications and participation (talks and posters) by group members at US conferences including the APS DAMOP meeting and international conferences. Refereed publications resulting from this project are listed and described in the attached pdf document.

**Honors and Awards:** The PI received an NSF CAREER award during the grant period.

**Protocol Activity Status:**

**Technology Transfer:** Nothing to Report

**PARTICIPANTS:**

**Participant Type:** Graduate Student (research assistant)
**Participant:** Ruwan Senaratne
**Person Months Worked:** 12.00 **Funding Support:**
Project Contribution:
National Academy Member: N

**Participant Type:** Graduate Student (research assistant)
**Participant:** Zach Geiger
**Person Months Worked:** 12.00 **Funding Support:**
Project Contribution:
National Academy Member: N

**Participant Type:** Graduate Student (research assistant)
**Participant:** Cora Fujiwara
**Person Months Worked:** 12.00 **Funding Support:**
Project Contribution:
National Academy Member: N

**Participant Type:** Graduate Student (research assistant)
**Participant:** Kevin Singh
**Person Months Worked:** 12.00 **Funding Support:**
Project Contribution:
National Academy Member: N

**Participant Type:** Graduate Student (research assistant)
**Participant:** Quinn Simmons
**Person Months Worked:** 12.00 **Funding Support:**
Project Contribution:
National Academy Member: N

**Participant Type:** Graduate Student (research assistant)
**Participant:** Misha Lipatov
**Person Months Worked:** 12.00 **Funding Support:**
Project Contribution:
National Academy Member: N

**Participant Type:** Graduate Student (research assistant)
**Participant:** Roshan Sajjad
**Person Months Worked:** 12.00 **Funding Support:**
Project Contribution:
National Academy Member: N

**Participant Type:** Graduate Student (research assistant)
**Participant:** Jeremy Tanlimco
**Person Months Worked:** 12.00 **Funding Support:**
Project Contribution:
National Academy Member: N

# RPPR Final Report
as of 07-May-2021

**Participant Type:** Undergraduate Student
**Participant:** Alec Cao
**Person Months Worked:** 12.00 **Funding Support:**
Project Contribution:
National Academy Member: N

**Participant Type:** Undergraduate Student
**Participant:** Max Prichard
**Person Months Worked:** 12.00 **Funding Support:**
Project Contribution:
National Academy Member: N

**Participant Type:** Undergraduate Student
**Participant:** Jack Pan
**Person Months Worked:** 12.00 **Funding Support:**
Project Contribution:
National Academy Member: N

**Participant Type:** PD/PI
**Participant:** David Weld
**Person Months Worked:** 6.00 **Funding Support:**
Project Contribution:
National Academy Member: N

**ARTICLES:**

**Publication Type:** Journal Article Peer Reviewed: Y **Publication Status:** 1-Published
**Journal:** Review of Scientific Instruments
Publication Identifier Type: DOI Publication Identifier: 10.1063/1.4907401
Volume: 8.6E+001 Issue: 2.0E+000 First Page #: 0
Date Submitted: Date Published:
Publication Location:
**Article Title:** Effusive atomic oven nozzle design using an aligned microcapillary array
**Authors:**
**Keywords:** atomic beam experimental methods collimation
**Abstract:** We present a simple and inexpensive design for a multichannel effusive oven nozzle which provides improved atomic beam collimation and thus extended oven lifetimes. Using this design, we demonstrate an atomic lithium source suitable for trapped-atom experiments. At a nozzle temperature of 525?°C, the collimated atomic beam flux directly after the nozzle is 1.2 × 1014 atoms/s with a peak beam intensity greater than 5.0 × 1016 atoms/s/sr. This suggests an oven lifetime of several decades of continuous operation.
**Distribution Statement:** 3-Distribution authorized to U.S. Government Agencies and their contractors
Acknowledged Federal Support:

# RPPR Final Report
as of 07-May-2021

**Publication Type:** Journal Article Peer Reviewed: Y **Publication Status:** 1-Published
**Journal:** Annalen der Physik
Publication Identifier Type: DOI Publication Identifier: 10.1002/andp.201700008
Volume: 529 Issue: 8 First Page #: 1700008
Date Submitted: 8/31/17 12:00AM Date Published: 8/1/17 7:00AM
Publication Location:
**Article Title:** Quantum Emulation of Extreme Non-Equilibrium Phenomena with Trapped Atoms
**Authors:** Shankari V. Rajagopal, Kurt M. Fujiwara, Ruwan Senaratne, Kevin Singh, Zachary A. Geiger, David M. \
**Keywords:** nonequilibrium quantum dynamics, quantum simulation
**Abstract:** Ultracold atomic physics experiments offer a nearly ideal context for the investigation of quantum systems far from equilibrium. We describe three related emerging directions of research into extreme non-equilibrium phenomena in atom traps: quantum emulation of ultrafast atom-light interactions, coherent phasonic spectroscopy in tunable quasicrystals, and realization of Floquet matter in strongly-driven lattice systems. We show that all three should enable quantum emulation in parameter regimes inaccessible in solid-state experiments, facilitating a complementary approach to open problems in non-equilibrium condensed matter.
**Distribution Statement:** 3-Distribution authorized to U.S. Government Agencies and their contractors
Acknowledged Federal Support: **Y**

**Publication Type:** Journal Article Peer Reviewed: Y **Publication Status:** 1-Published
**Journal:** Physical Review Letters
Publication Identifier Type: DOI Publication Identifier: 10.1103/PhysRevLett.120.213201
Volume: 120 Issue: 21 First Page #:
Date Submitted: 8/31/18 12:00AM Date Published: 5/1/18 7:00AM
Publication Location:
**Article Title:** Observation and Uses of Position-Space Bloch Oscillations in an Ultracold Gas
**Authors:** Zachary A. Geiger, Kurt M. Fujiwara, Kevin Singh, Ruwan Senaratne, Shankari V. Rajagopal, Mikhail Li
**Keywords:** bloch oscillations, quantum dynamics
**Abstract:** We report the observation and characterization of position-space Bloch oscillations using cold atoms in a tilted optical lattice. While momentum-space Bloch oscillations are a common feature of optical lattice experiments, the real-space center-of-mass dynamics are typically unresolvable. In a regime of rapid tunneling and low force, we observe real-space Bloch oscillation amplitudes of hundreds of lattice sites, in both ground and excited bands. We demonstrate two unique capabilities enabled by tracking of Bloch dynamics in position space: measurement of the full position-momentum phase-space evolution during a Bloch cycle, and direct imaging of the lattice band structure. These techniques, along with the ability to exert long-distance coherent control of quantum gases without modulation, may open up new possibilities for quantum control and metrology.
**Distribution Statement:** 3-Distribution authorized to U.S. Government Agencies and their contractors
Acknowledged Federal Support: **Y**

# RPPR Final Report
as of 07-May-2021

**Publication Type:** Journal Article Peer Reviewed: Y **Publication Status:** 1-Published
**Journal:** Nature Communications
Publication Identifier Type: DOI Publication Identifier: 10.1038/s41467-018-04556-3
Volume: 9 Issue: 1 First Page #:
Date Submitted: 8/31/18 12:00AM Date Published: 5/1/18 12:00AM
Publication Location:
**Article Title:** Quantum simulation of ultrafast dynamics using trapped ultracold atoms
**Authors:** Ruwan Senaratne, Shankari V. Rajagopal, Toshihiko Shimasaki, Peter E. Dotti, Kurt M. Fujiwara, Kevin
**Keywords:** quantum dynamics, ultrafast
**Abstract:** Ultrafast electronic dynamics are typically studied using pulsed lasers. Here we demonstrate a complementary experimental approach: quantum simulation of ultrafast dynamics using trapped ultracold atoms. Counter-intuitively, this technique emulates some of the fastest processes in atomic physics with some of the slowest, leading to a temporal magnification factor of up to 12 orders of magnitude. In these experiments, time-varying forces on neutral atoms in the ground state of a tunable optical trap emulate the electric fields of a pulsed laser acting on bound charged particles. We demonstrate the correspondence with ultrafast science by a sequence of experiments: nonlinear spectroscopy of a many-body bound state, control of the excitation spectrum by potential shaping, observation of sub-cycle unbinding dynamics during strong few-cycle pulses, and direct measurement of carrier-envelope phase dependence of the response to an ultrafast-equivalent pulse. These results establish...
**Distribution Statement:** 3-Distribution authorized to U.S. Government Agencies and their contractors
Acknowledged Federal Support: **Y**

**Publication Type:** Journal Article Peer Reviewed: Y **Publication Status:** 1-Published
**Journal:** New Journal of Physics
Publication Identifier Type: DOI Publication Identifier: 10.1088/1367-2630/aacb5a
Volume: 20 Issue: 6 First Page #: 063027
Date Submitted: 8/31/18 12:00AM Date Published: 6/1/18 12:00AM
Publication Location:
**Article Title:** Experimental realization of a relativistic harmonic oscillator
**Authors:** Kurt M Fujiwara, Zachary A Geiger, Kevin Singh, Ruwan Senaratne, Shankari V Rajagopal, Mikhail Lipa
**Keywords:** bloch oscillations, lattice dynamics, band structure
**Abstract:** We report the observation and characterization of position-space Bloch oscillations using cold atoms in a tilted optical lattice. While momentum-space Bloch oscillations are a common feature of optical lattice experiments, the real-space center-of-mass dynamics are typically unresolvable. In a regime of rapid tunneling and low force, we observe real-space Bloch oscillation amplitudes of hundreds of lattice sites, in both ground and excited bands. We demonstrate two unique capabilities enabled by tracking of Bloch dynamics in position space: measurement of the full position-momentum phase-space evolution during a Bloch cycle, and direct imaging of the lattice band structure. These techniques, along with the ability to exert long-distance coherent control of quantum gases without modulation, may open up new possibilities for quantum control and metrology.
**Distribution Statement:** 3-Distribution authorized to U.S. Government Agencies and their contractors
Acknowledged Federal Support: **Y**

**DISSERTATIONS:**

**Publication Type:** Thesis or Dissertation
**Institution:** University of California, Santa Barbara
Date Received: 31-Aug-2018 Completion Date: 6/7/18 12:34AM
**Title:** Quantum Simulation of Strongly-Driven Systems Using Ultracold Lithium and Strontium
**Authors:** Ruwan Senaratne
Acknowledged Federal Support: **Y**

# RPPR Final Report
as of 07-May-2021

**Publication Type:** Thesis or Dissertation
**Institution:** University of California, Santa Barbara
Date Received: 31-Aug-2018 Completion Date: 12/14/17 4:00PM
**Title:** An Apparatus for Dynamical Quantum Emulation Using Ultracold Lithium
**Authors:** Zachary Geiger
Acknowledged Federal Support: **Y**

**Partners**

,

I certify that the information in the report is complete and accurate:
Signature: David Minot Weld
Signature Date: 5/6/21 6:23PM

# Final Report

Overarching goals of this project included demonstration of dynamic stabilization in modulated lattices, measurement of the effects of interactions on quantum chaotic behavior, measurement of quench dynamics, experimental probes of quantum thermalization, and probes of topological transport dynamics. The apparatus constructed during the grant period to enable pursuit of these goals is shown in Fig. 1. Experimental results have addressed all of these goals, as well as some targets of opportunity that have arisen during our study of nonequilibrium quantum dynamics. Published results include the first observation of position-space Bloch oscillations, the first quantum simulator of ultrafast dynamics, the experimental realization of a relativistic harmonic oscillator in an excited band of a lattice, the demonstration of quantum control of long-range transport by Floquet band engineering, an experimental demonstration of Floquet prethermalization in driven quantum systems, a study of nonexponential decay in Floquet-Bloch bands, an exploration of phasonic spectroscopy in a tunable quantum quasicrystal, and measurements of transport controlled by Poincare orbit topology in a driven inhomogeneous lattice gas. Details of key results are given below; related figures appear after the text in this document.

**Observation of position-space Bloch oscillations (see also Figs. 2-5 below)**. It was predicted nearly a century ago that applying a constant force to quantum particles in a lattice would give rise to an oscillatory motion known as a Bloch oscillation. The resultant localization is a fundamental feature of coherent transport in a lattice. We have experimentally observed and characterized position-space Bloch oscillations in an ultracold lattice-trapped lithium gas. Previously these oscillations have been inferred only from momentum-space measurements. This result realizes the original conception of Bloch oscillations and opens a new avenue of investigation into fundamental features of quantum transport dynamics. We demonstrated two fundamentally new techniques which are enabled by position-space Bloch oscillations: a measurement of the full position-momentum phase space trajectory during a Bloch oscillation, and direct imaging of band structure. Together with the demonstration of long-range dissipation-free transport control without modulation, these results open up new possibilities for quantum control and metrology. The work was published in *Physical Review Letters* as an Editor's Suggestion [1], and highlighted with a synopsis in *Physics.*

**Cold atom quantum simulation of ultrafast dynamics (see also Figs. 6-7 below).** Pulsed lasers can now probe the behavior of electrons inside atoms at timescales smaller than a femtosecond, but applying this capability to unlock new technologies requires major advances in understanding and control of the ultrafast dynamics of quantum mechanical systems far from equilibrium. My group demonstrated a new experimental approach to this central goal of ultrafast science: quantum simulation in an artificial atom or molecule made from trapped ultracold atoms. Counter-intuitively, this approach probes some of the fastest processes in atomic physics using some of the slowest. The resulting temporal magnification factor of more than a trillion allows detailed study and control of ultrafast-equivalent dynamics on subcycle timescales in regimes hard or impossible to reach with pulsed lasers. In an article in *Nature Communications* [2], we present measurements of the effects of pulse amplitude and carrier-envelope phase on ultrafast-equivalent sub-cycle unbinding dynamics. This work establishes a direct experimental connection between two vibrant but largely unconnected subfields of atomic physics: ultrafast science and ultracold atoms.

**Experimental realization of a relativistic harmonic oscillator (see also Figs. 8-9 below).** The harmonic oscillator has been a central concept in physics and technology since Galileo's observations of constant-period pendulum motion. The advent of special relativity suggested a simple question: what happens when the velocity of a harmonic oscillator approaches the speed of light? While theoretical treatments of the relativistic harmonic oscillator have been discussed for decades, it has proven surprisingly resistant to physical realization. In a paper published in *New Journal of Physics* [3] we report the first dynamical experimental realization of a harmonic oscillator in the relativistic regime, using ultracold atoms in an excited band of an optical lattice. Measurements of relativistic worldline dynamics, anharmonicity, and dephasing

demonstrate excellent quantitative agreement with exact relativistic theories.

**Transport in Floquet-Bloch bands (see also Figs. 10-13 below).** Floquet band engineering in driven lattices may hold the key to new device types, unexplored techniques for ultrafast transport of energy and information, and dynamical tools for controlling and probing condensed matter. In a recent experiment published in *Phys. Rev. Letters*, my group demonstrated Floquet band engineering of long-range transport and direct imaging of Floquet-Bloch bands in an amplitude-modulated optical lattice [4]. We used Floquet hybridization in the presence of an applied force to generate coherent transport over thousands of lattice sites, switch on and off Bloch oscillations, tune the band dispersion by manipulating drive parameters, and image Floquet-Bloch band structure. These results open a path to unexplored applications of Floquet engineering, quantum emulation of ultrafast multi-band electronic dynamics, and Floquet-enhanced metrology, and realize an important synergy with the goals of our ARO MURI project on anyon synthesis.

**Floquet prethermalization (see also Figs. 14-18 below).** We have successfully conducted a detailed experimental investigation of Floquet prethermalization in strongly driven quantum systems, using a double-quench protocol. A major scientific motivation for this work was that while strong driving of many-body quantum systems can engineer new material properties, it can also cause destructive heating. Floquet prethermalization theoretically allows drive-tunable states to persist over useful time scales. We have experimentally characterized the Floquet phase diagram of tunably-interacting lithium atoms in an optical lattice amplitude-modulated at up to a thousand percent. We observed a delocalization crossover which agrees quantitatively with predictions from a periodic generalized Gibbs ensemble. Measuring the full dynamical evolution reveals a prethermal plateau whose long-time fate depends on interaction strength and drive parameters. At the highest drive frequencies and interaction strengths the prethermal plateau is followed by root-time heating; this mysterious behavior has also been predicted by numerical theories but the mechanism is not understood. The experimental observation of Floquet prethermalization opens new possibilities for drive-based engineering of many-body quantum states. This work was published in *Phys. Rev. X* [5].

**Phasonic driving (see also Figs. 19-21 below).** We have demonstrated the first phasonic spectroscopy of a quasicrystal, achieved by experimentally measuring the frequency-dependent response to phasonic driving of a quantum gas in a quasiperiodic optical lattice. Phasonic degrees of freedom are unique to quasiperiodic structures, and play a central role in poorly-understood properties of quasicrystals from excitation spectra to wavefunction statistics to electronic transport. However, phasons are extremely challenging to access dynamically in the solid state due to their complex long-range character and the effects of disorder and strain. We observe that strong phasonic driving produces a nonperturbative high-harmonic response strikingly different from the effects of standard dipolar driving, giving rise to a plateau of high-order multiphoton transitions in the quasicrystal. Tuning from a crystal to a quasicrystal, we have identified spectroscopic signatures of quasiperiodicity and interactions and mapped the emergence of a multifractal energy spectrum, opening a path to direct imaging of the Hofstadter butterfly. This work was published in *Phys. Rev. Letters* [6].

**Probing non-exponential decay with Floquet-Bloch bands (see also Figs. 22-25 below).** Exponential decay laws describe systems ranging from unstable nuclei to fluorescent molecules, in which the probability of jumping to a lower-energy state in any given time interval is static and history-independent. These decays, involving only a metastable state and fluctuations of the quantum vacuum, are the most fundamental nonequilibrium process and provide a microscopic model for the origins of irreversibility. Despite the fact that the apparently universal exponential decay law has been precisely tested in a variety of physical systems, it is a surprising truth that quantum mechanics *requires* that spontaneous decay processes have nonexponential time dependence at both very short and very long times. The long-time deviations have never been observed at the single-emitter level. My group recently proposed the use of Bose condensates in Floquet-Bloch bands as a probe of long-time nonexponential decay, and experimentally demonstrated a

key element: tunable decay between quasi-energy bands in a driven optical lattice. This work is reported in an invited publication in a special issue of *Zeitschrift für Naturforschung A* [7].

**Poincaré orbit topology and transport dynamics (see also Figs. 26-29 below).** Almost 350 years ago, Newton explained that a constant force creates constant acceleration. A century ago, Bloch and Zener applied the new discipline of quantum mechanics to show that a steady force on electrons in a crystal lattice leads instead to an oscillatory response, now called a Bloch oscillation. A decade ago, cold atom experiments generalized this behavior to the case of a time-varying force, which produces an interplay of multiple oscillations. My group recently reported the next step in this line of exploration, experimentally measuring the response of atoms in a time-varying lattice to a spatially nonuniform force. The interplay between position-dependent Bloch oscillations and a time-dependent band structure gives rise to a rich variety of transport dynamics, from directed charge pumping to a rapid tearing-apart of the wave function. Strikingly, a unified understanding of these quantum dynamical phenomena can be obtained using concepts from nonlinear dynamics: a topological classification of stroboscopic Poincaré orbits controls the transport behavior. These results open new directions in the field of dynamical quantum engineering. The results are published in *Physical Review Research* [8].

**Related activities.** PI Weld is the co-design lead for quantum simulation for the new DOE-supported "Quantum Science Center," the lead coordinator for a KITP program on "Revealing Emergent Many-Body Phenomena with Spatiotemporal Control," and the lead PI for the Broadly-tunable Illumination Facility for Research, Outreach, Scholarship, and Training (BIFROST), a multi-user ARO-suported light source facility supplying tunable spectroscopy-grade light throughout the visible and near-infrared range to ten research and teaching labs in Broida Hall.

---


[1] Zachary A. Geiger, Kurt M. Fujiwara, Kevin Singh, Ruwan Senaratne, Shankari V. Rajagopal, Mikhail Lipatov, Toshihiko Shimasaki, Rodislav Driben, Vladimir V. Konotop, Torsten Meier, and David M. Weld. Observation and uses of position-space Bloch oscillations in an ultracold gas. *Phys. Rev. Lett.*, 120:213201, May 2018.

[2] Ruwan Senaratne, Shankari V. Rajagopal, Toshihiko Shimasaki, Peter E. Dotti, Kurt M. Fujiwara, Kevin Singh, Zachary A. Geiger, and David M. Weld. Quantum simulation of ultrafast dynamics using trapped ultracold atoms. *Nature Communications*, 9(1):2065, 2018.

[3] Kurt M Fujiwara, Zachary A Geiger, Kevin Singh, Ruwan Senaratne, Shankari V Rajagopal, Mikhail Lipatov, Toshihiko Shimasaki, and David M Weld. Experimental realization of a relativistic harmonic oscillator. *New Journal of Physics*, 20(6):063027, 2018.

[4] C. J. Fujiwara, Kevin Singh, Zachary A. Geiger, Ruwan Senaratne, Shankari V. Rajagopal, Mikhail Lipatov, and David M. Weld. Transport in Floquet-Bloch bands. *Phys. Rev. Lett.*, 122:010402, Jan 2019.

[5] K. Singh, C. J. Fujiwara, Z. A. Geiger, E. Q. Simmons, M. Lipatov, A. Cao, P. Dotti, S. V. Rajagopal, R. Senaratne, T. Shimasaki, M. Heyl, A. Eckardt, and D. M. Weld. Quantifying and controlling prethermal nonergodicity in interacting Floquet matter. *Phys. Rev. X*, 9:041021, Oct 2019.

[6] Shankari V. Rajagopal, Toshihiko Shimasaki, Peter Dotti, Mantas Raciunas, Ruwan Senaratne, Egidijus Anisimovas, André Eckardt, and David M. Weld. Phasonic spectroscopy of a quantum gas in a quasicrystalline lattice. *Phys. Rev. Lett.*, 123(223021), 2019.

[7] Alec Cao, Cora J. Fujiwara, Roshan Sajjad, Ethan Q. Simmons, Eva Lindroth, and David Weld. Probing nonexponential decay in Floquet–Bloch bands. *Zeitschrift für Naturforschung A*, 75(5):443, 2020.

[8] Alec Cao, Roshan Sajjad, Ethan Q. Simmons, Cora J. Fujiwara, Toshihiko Shimasaki, and David M. Weld. Transport controlled by poincaré orbit topology in a driven inhomogeneous lattice gas. *Phys. Rev. Research*, 2:032032, Aug 2020.

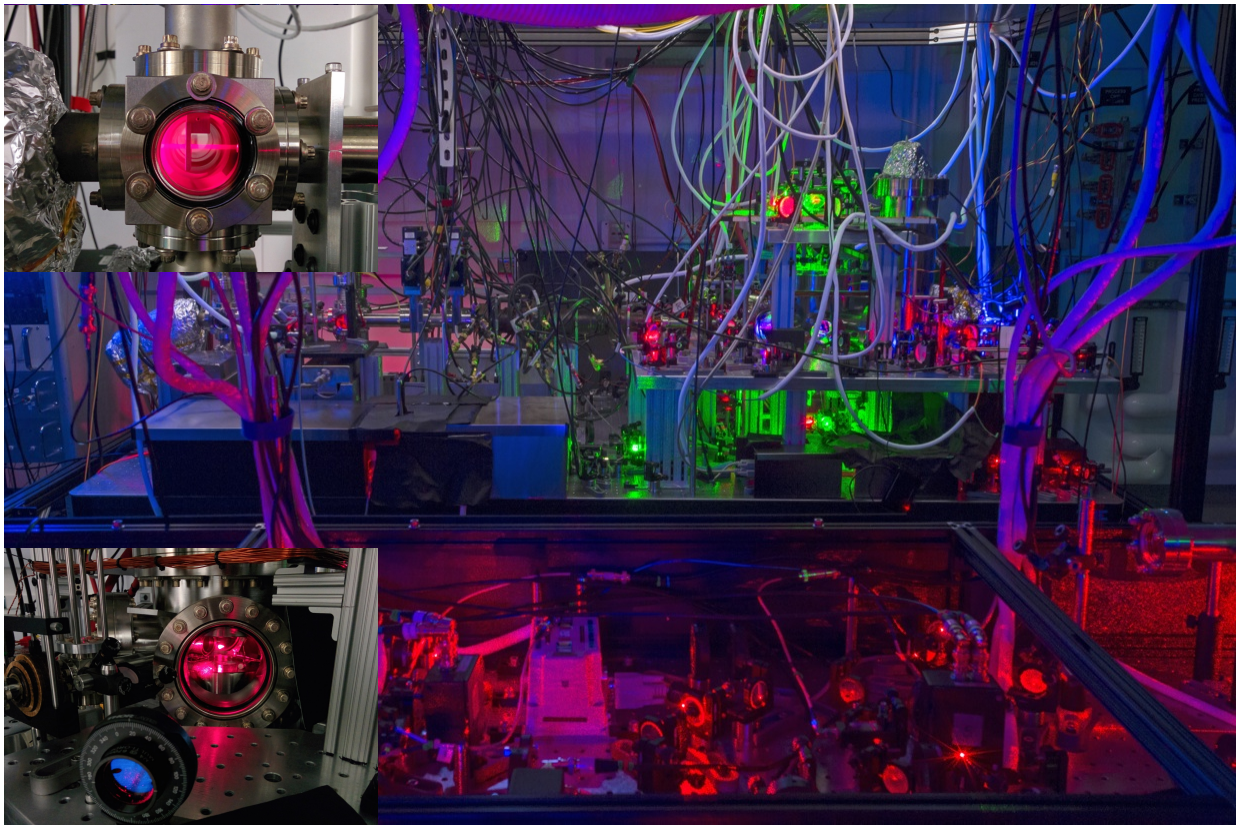

FIG. 1: Ultracold lithium apparatus in the Weld lab at UCSB, constructed to enable the goals of the PECASE project. Red light is from the 671nm cooling and trapping laser, green light is from the 532nm optical plug beam for the quadrupole trap, and blue light is from the non-coherent 400nm source used to prevent lithium deposition on the Zeeman slower window. Top and bottom insets show the atomic beam and magneto-optical trap, respectively.

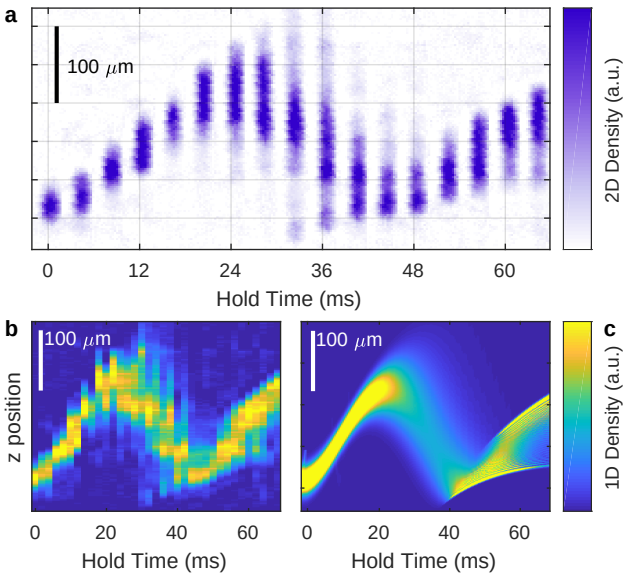


FIG. 2: Position-space Bloch oscillations. **(a)** Time sequence of in-situ absorption images of atoms in a 5.4 $E_R$-deep optical lattice subjected to a force corresponding to a Bloch frequency of 21.1 Hz. Each image corresponds to an individual experimental run with the indicated hold time. **(b)** Measured evolution of integrated density distribution as a function of axial position during a Bloch oscillation. **(c)** Numerical GPE prediction for (b), using the split-step Fourier method. Asymmetrical width variation is due to force inhomogeneity.

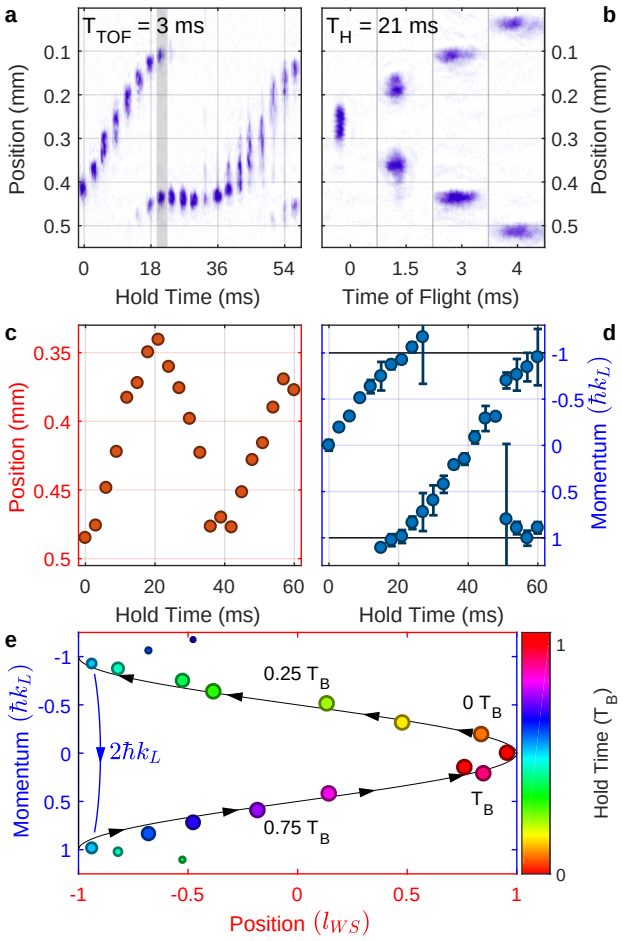


FIG. 3: Phase-space evolution during a Bloch oscillation. Here $J = 1.55$ kHz and $F = 23$ Hz. **(a)** Absorption images of the atomic distribution after a 3 ms time of flight. The distribution at each hold time is a convolution of initial quasimomentum and position. **(b)** Absorption images after varying times of flight, for a hold time of 21 ms. The initial quasimomentum can be extracted via a linear fit. **(c,d)** Ensemble position and momentum versus time during a Bloch oscillation. Where multiple momentum peaks can be distinguished, both are plotted. **(e)** Combining (c) and (d) yields the phase space evolution of the ensemble during the first Bloch period $T_B = 1/f_B$. Color map corresponds to the hold time in units of $T_B$. Where multiple momentum peaks can be distinguished, both are plotted with symbol size indicating relative atom number. At $0.5T_B$, Bragg scattering is observed as a discontinuity of $2\hbar k_L$ in the measured momentum distribution.

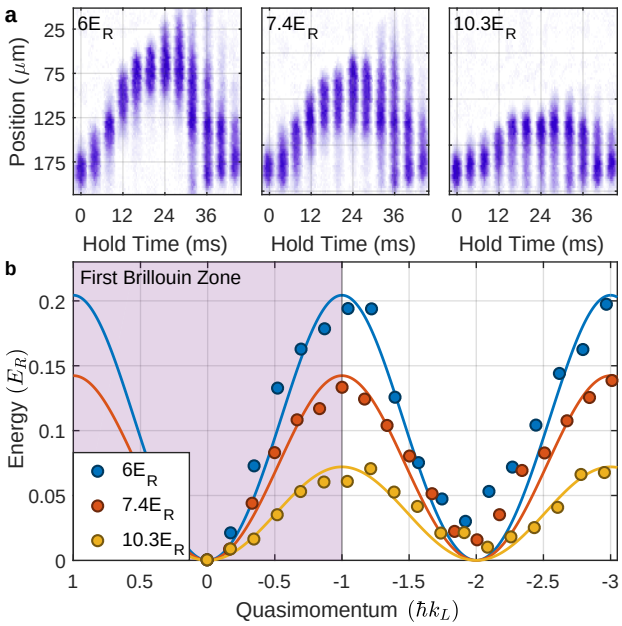


FIG. 4: Band imaging with position-space Bloch oscillations. **(a)** Time-series images of atomic ensembles undergoing Bloch oscillations in lattice depths of 6 $E_R$, 7.4 $E_R$, and 10.3 $E_R$. **(b)** Measured band structure $E(k)$ for the three lattice depths (circles), determined by scaling the measured center positions from (a). Lines show independently-calculated band structures with no adjustable parameters.

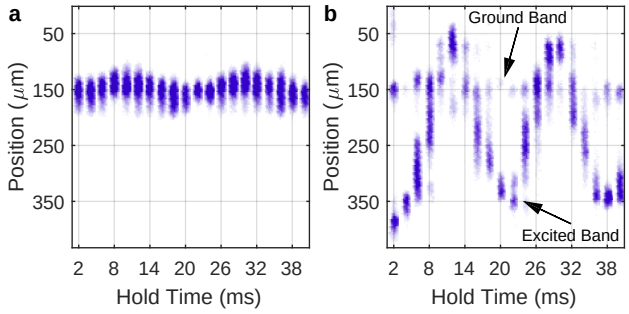


FIG. 5: Position-space Bloch oscillations in an excited band. The lattice depth is set to $9.5E_R$ and the Bloch frequency to $50.7$ Hz. **(a)** Time-series absorption image of ground-band Bloch oscillations. **(b)** Time-series image of Bloch oscillations in the first excited band, which are characterized by the same frequency as ground-band oscillations, but exhibit a significantly larger amplitude due to the larger bandwidth. Also visible is a remnant fraction of atoms in the ground band, due to imperfect excitation. These Bloch-oscillate independently.

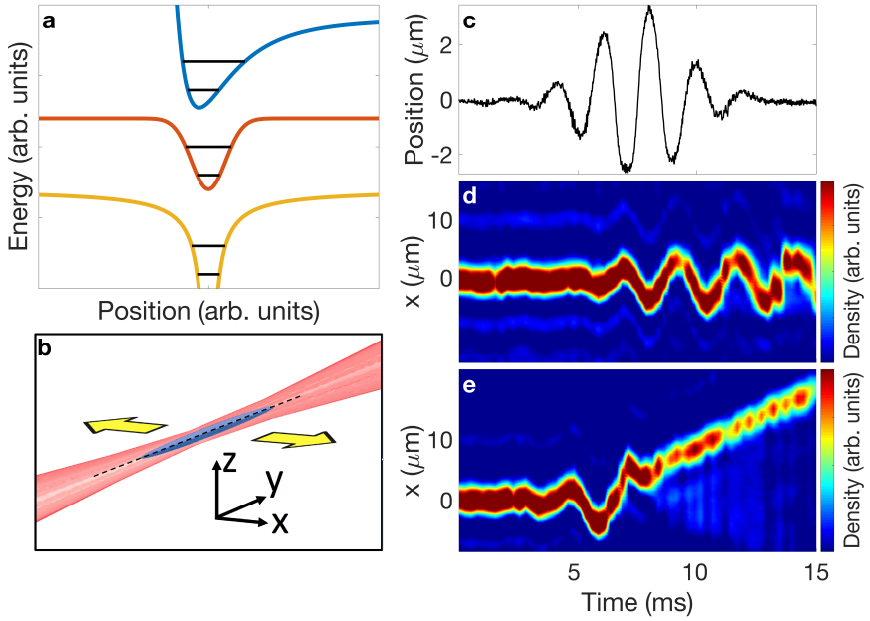


FIG. 6: **Quantum simulation of ultrafast dynamics. a:** Schematic bound states of Lennard-Jones, Gaussian, and $1/r$ potentials (offset for clarity). **b:** Diagram of optical trap (red), which is shaken in the $\hat{\mathbf{x}}$ direction to generate inertial forces on the condensate (blue). **c:** Measured trap position $\alpha(t)$ during a pulse. **d:** Response to a weak pulse. Colourmap shows density distribution after time-of-flight as a function of time. Pulse carrier frequency is 450 Hz, pulse envelope width is 3.76 ms, pulse amplitude is 0.6 $\mu$m, and carrier-envelope phase is 0. **e:** Response to a stronger pulse. Unbinding occurs near 8 ms, after which the atoms propagate with constant velocity. Pulse amplitude is 2.4 $\mu$m. All other pulse parameters are identical to those in **d**.

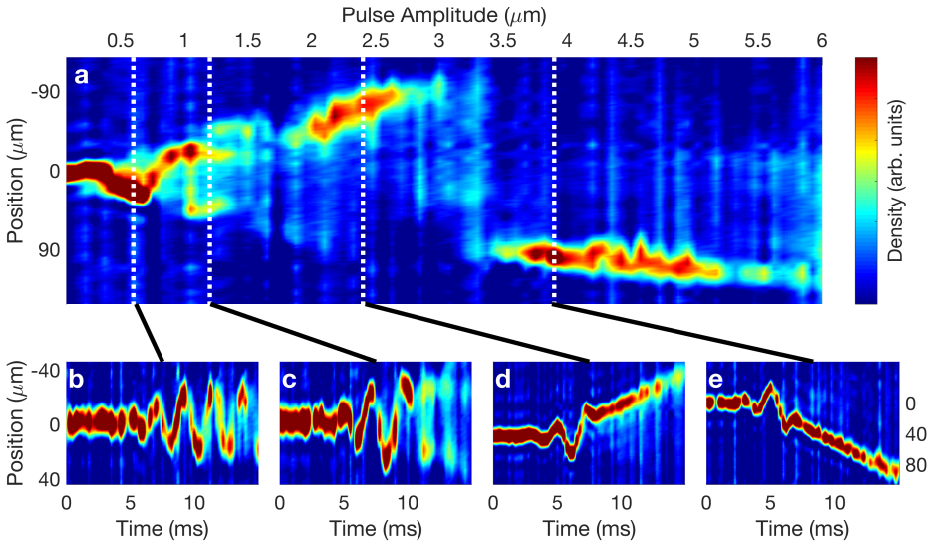


FIG. 7: **Dependence of unbinding dynamics on pulse amplitude. a:** Integrated spatial density distribution after application of a near-resonant 480 Hz pulse with $\tau = 3.76$ ms and $\phi = 0$ followed by 2 ms time-of-flight, versus pulse amplitude $A$. **b-e:** Integrated spatial density distribution versus time during pulses with the indicated amplitude. Panels **d** and **e** have an expanded $y$-axis (indicated at right) to track the unbound atoms. Note the momentum of the unbound atoms changing sign as the pulse amplitude increases.

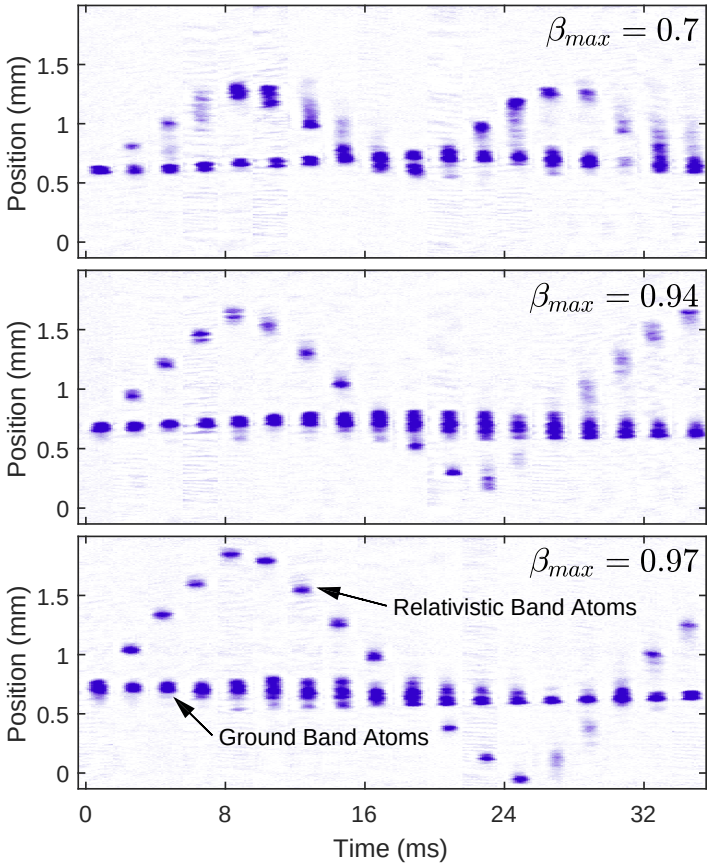


FIG. 8: Measured trajectories of relativistic harmonic oscillators. Each panel shows a time sequence of in-situ absorption images of a non-interacting atomic cloud with population in the first and third bands of an optical lattice. Third-band atoms trace out relativistic harmonic oscillator worldlines of increasing amplitude and period. Ground-band atoms Bloch oscillate around their original position, and are irrelevant to the relativistic dynamics. The maximum value of $\beta = v/c$ indicated in each panel was attained by loading the third band at varying quasimomenta, using excitation frequencies of (from top to bottom) 137, 170, and 210 kHz and corresponding hold times before excitation of 0 ms, 8 ms, and 16 ms.

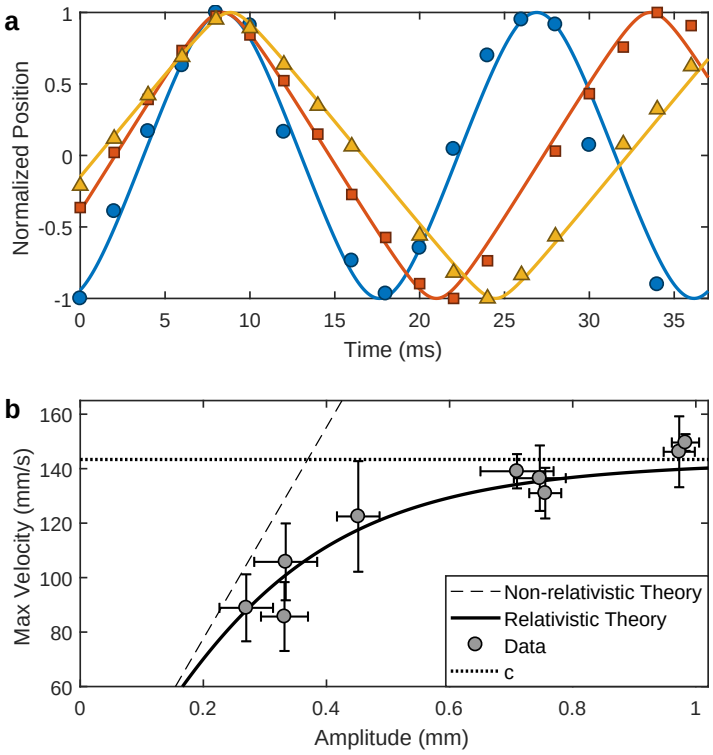


FIG. 9: Measuring relativistic harmonic oscillator dynamics. **a:** Comparison of measured and theoretical trajectories. Measured normalized mean atomic position versus time for $\beta_{\max} = 0.7$ (blue circles), 0.94 (red squares), and 0.97 (yellow triangles). Solid lines show theoretically predicted evolution with no adjustable fit parameters. **b:** Amplitude-velocity relation of the relativistic harmonic oscillator. Points show measured peak velocity versus measured amplitude. Amplitude error bars indicate the $1/e$ ensemble radius and velocity error bars indicate estimated uncertainty of numerical differentiation. Lines show the non-relativistic expectation (dashed), the exact relativistic prediction (solid), and the effective speed of light (dotted).

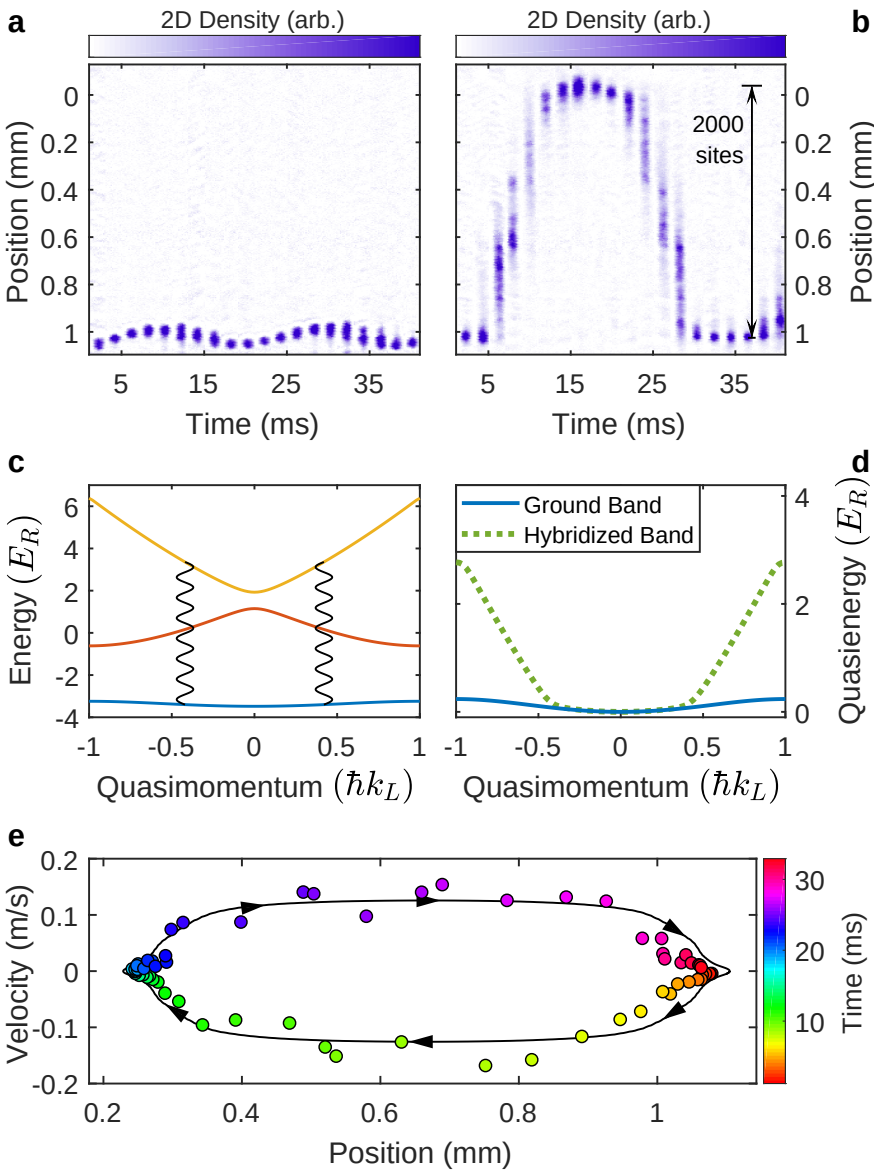


FIG. 10: Rapid long-range transport in a Floquet-Bloch band, from [4]. **(a)** Time sequence of images of a condensate in the ground band with lattice depth $V_0 = 5.4\ E_R$. A force of $6{\times}10^{-26}$ N per atom induces Bloch oscillations. **(b)** Time sequence of images of a condensate in a $(0, 2)$ hybridized Floquet-Bloch band created via amplitude modulation with $\nu = 170$ kHz and $\alpha = 0.2$, with the same initial force as in (a). Note the rapid cyclic high-fidelity transport across the trap. **(c)** Unmodified band structure. Vertical rippled lines indicate band coupling at the hybridizing quasimomentum for this modulation frequency. **(d)** Calculated dispersion of the unmodified ground band (solid) and hybridized Floquet-Bloch band (dashed). **(e)** Position-velocity evolution in the same hybrid band as (b) with an initial force of $5{\times}10^{-26}$ N per atom. Solid line is theory; points are data, taken at equally-spaced times.

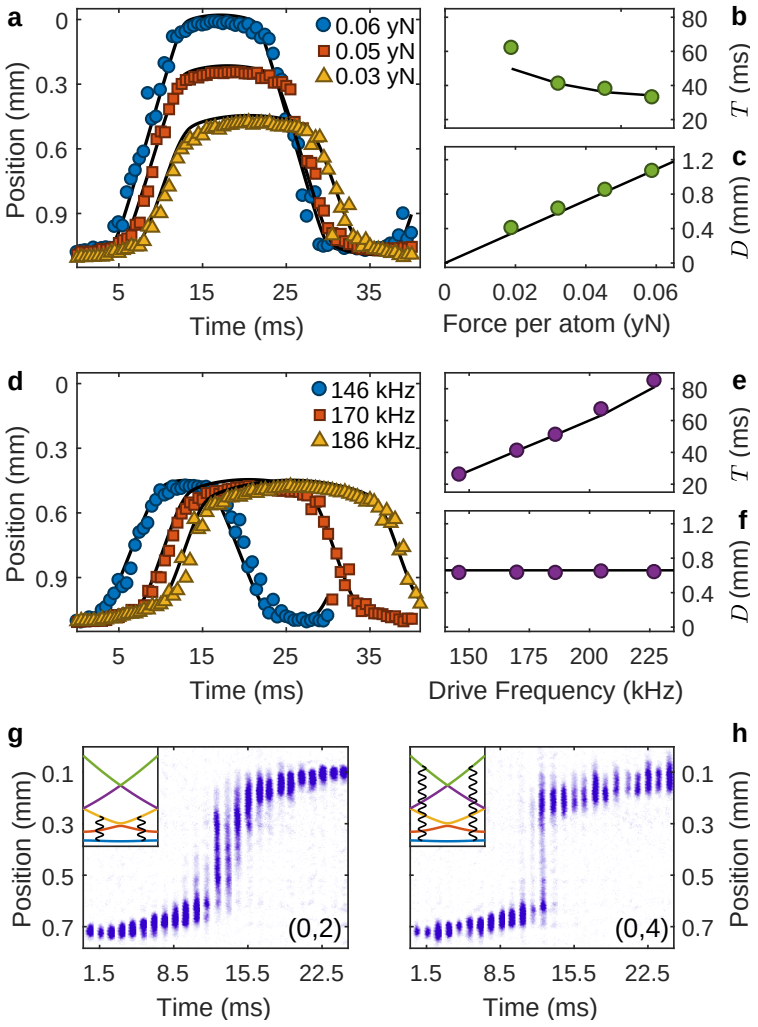


FIG. 11: Tunable transport in Floquet-Bloch bands. Panels a-g show measurements in a $(0, 2)$ hybrid band with $\alpha = 0.2$. **(a)** Atomic center-of-mass position versus time for constant drive frequency $\nu = 170$ kHz and varying initial force as indicated in the legend. In panels a-f, theoretical expectations from the calculated Floquet-Bloch band structure are plotted as solid lines, with no fit parameters. **(b,c)** Transport period and total transport distance as a function of initial force. **(d)** Atomic position versus time for a constant initial force per atom $F = 3.3 \times 10^{-26}$ N and varying drive frequency as indicated in the legend. **(e,f)** Transport period and total transport distance as a function of drive frequency $\nu$. **(g)** Time sequence of position-space distribution in a $(0, 2)$ Floquet-Bloch band with $\nu = 186$ kHz and $\alpha = 0.2$. **(h)** Time sequence of position-space distribution in a $(0, 4)$ hybrid Floquet-Bloch band with $\nu = 530$ kHz and $\alpha = 1$. Insets in (g) and (h) show hybridization schematic in the static band structure.

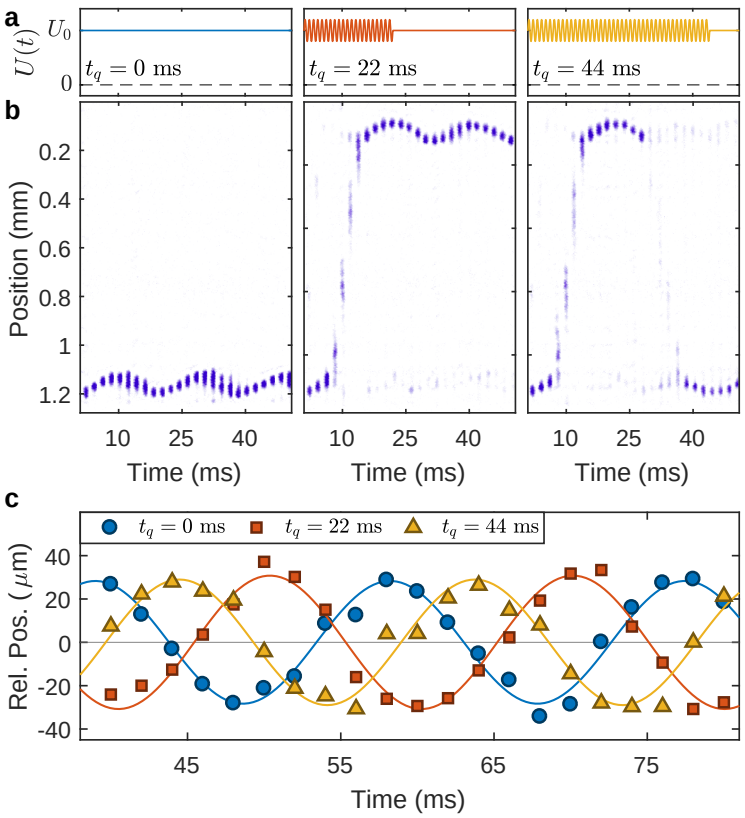


FIG. 12: Transport control via Floquet quenches. **(a)** Schematic of the quench protocol for modulation times of 0, 22, and 44 ms. **(b)** Time sequence of images of the atomic ensemble undergoing the three quench protocols. **(c)** Relative position evolution of the atomic ensemble after all quenches. Solid lines are sinusoidal fits. The consistent frequency and amplitude of Bloch oscillations after all quenches demonstrates the coherent nature of the transport.

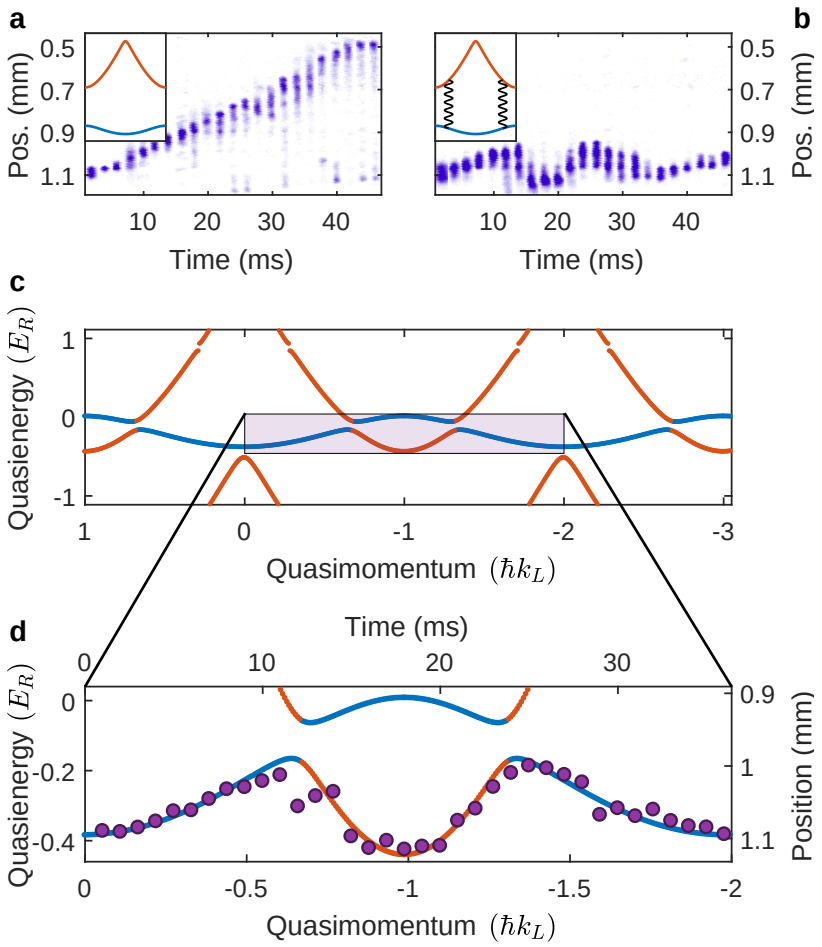


FIG. 13: Imaging a Floquet-Bloch band. **(a)** Time sequence of images of atoms undergoing ballistic transport in a static band with reduced lattice depth $V_0 = 3.6\ E_R$. Inset is the calculated band structure. **(b)** Evolution in a $(0, 1)$ hybrid Floquet-Bloch band with $\nu = 56$ kHz, $\alpha = 0.25$, and the same lattice depth as (a). Inset is the static band structure with rippled lines indicating the resonant coupling. **(c)** Calculated quasienergy spectrum in the extended zone for the $(0, 1)$ scheme described in (b). Color corresponds to the static band with maximal probability overlap with the Floquet state according to the band colors in (a). Shaded region corresponds to the mapped part of the Floquet band in (d). **(d)** Comparison of the real-space evolution in (b) to the Floquet spectrum in (c) according to the mapping with no fit parameters. The atomic motion images the Floquet-Bloch band dispersion.

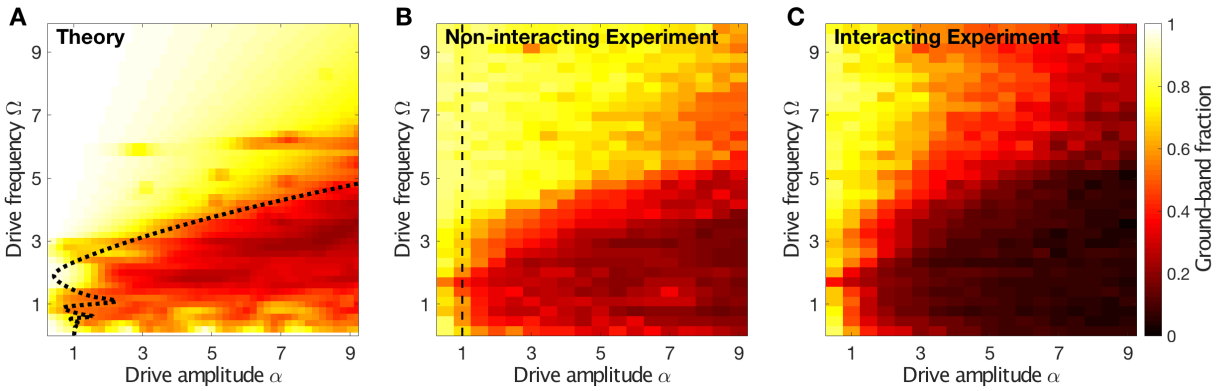


FIG. 14: Mapping the prethermal state in the space of drive parameters. **A:** Theoretical map of the projected static ground band occupation fraction for a non-interacting periodic Gibbs ensemble, as a function of normalized drive frequency $\Omega$ and normalized drive amplitude $\alpha$. Dotted line shows classical stability boundary of the equivalent driven pendulum. **B:** Experimental measurement of normalized population in the center of the lowest band after a 500 $\mu$s hold of a non-interacting quantum gas in a modulated optical lattice, as a function of the same parameters. The $\alpha > 1$ region to the right of the vertical dashed line is inaccessible without the sign-changing amplitude modulation introduced in this work. **C:** Same measurement as B, but in the presence of interatomic interactions ($s$-wave scattering length 30 nm). Colorbar and axes are the same for all three panels.

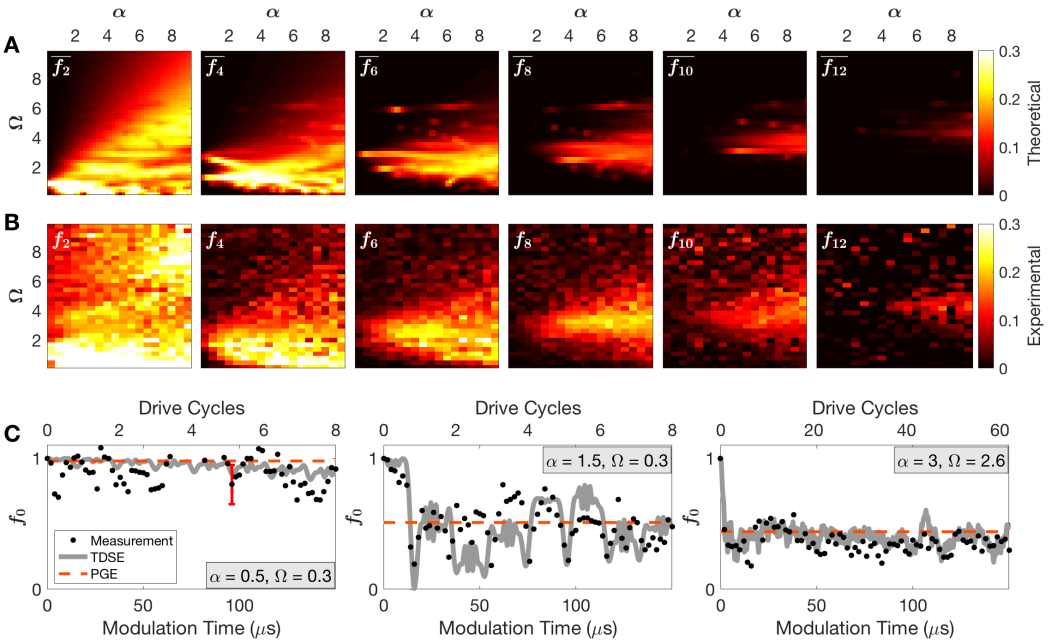


FIG. 15: Characterizing the prethermal periodic Gibbs ensemble. **A:** PGE prediction for occupation of excited even bands as a function of drive parameters $\alpha$ and $\Omega$. **B:** Measured atom number fraction in the central 40% of the same bands. All axes and colorbars are the same as for the theory panels. **C:** Measured $f_0$ versus modulation time for the first 150 $\mu$s of the drive, for three different values of $(\alpha, \Omega)$ all for vanishing interactions. Dashed line shows PGE prediction, solid line shows TDSE prediction of the fluctuating evolution of a spatially homogeneous non-interacting system. Each point represents a single run; error bar shows representative estimated fractional error due to shot-to-shot number fluctuation. For these data, the optical lattice is immediately quenched back to the initial 10 $E_R$ static lattice at the indicated modulation time and then band-mapped.

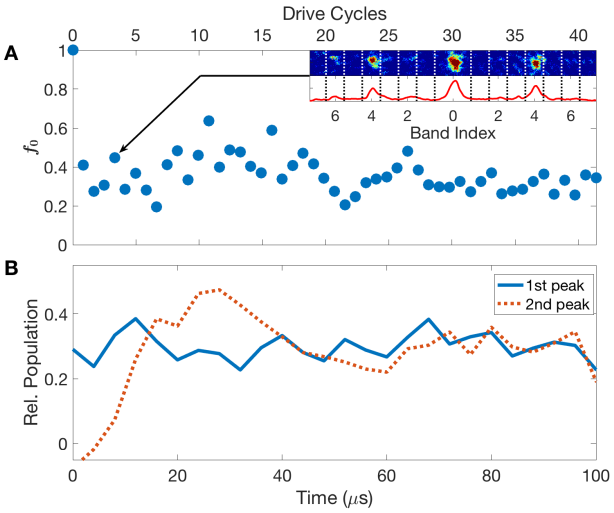


FIG. 16: Entering the prethermal state. **A:** Normalized ground band occupation $f_0$ as a function of time during modulation with $\alpha = 3$, $\Omega = 2.6$, $a = 0$. The system attains the prethermal value of $f_0$ on time scales comparable to a single drive cycle. These data are reproduced from the rightmost panel of Fig. 2C to facilitate direct comparison with Fig. 3B. Inset shows a sample bandmapped image and its column integration for the indicated data point, with Brillouin zone boundaries and band indices labeled. **B:** Population fraction in diffracted peaks after diabatic lattice snapoff, as a function of time during the same drive. $x$ axes are the same for the two plots. Gradual attainment of the prethermal steady-state is apparent in the settling of the second-peak population.

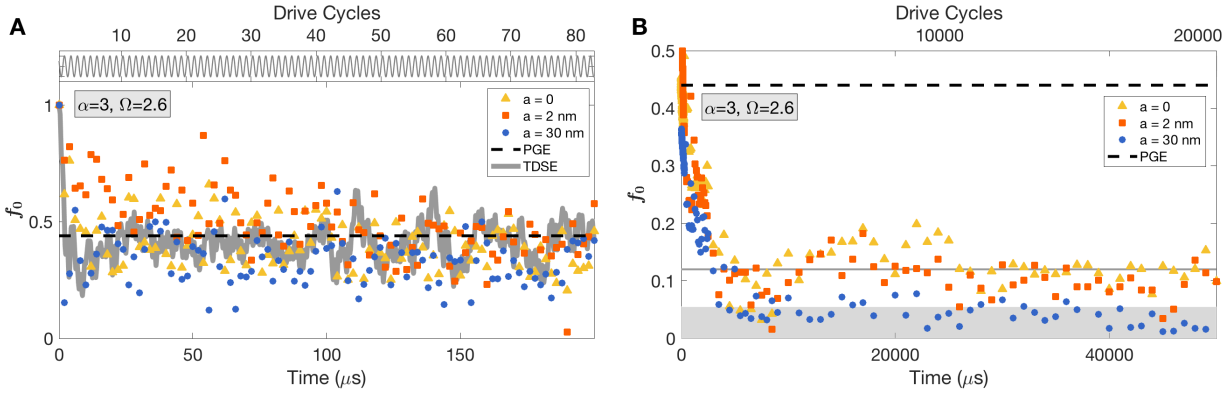


FIG. 17: Effect of interaction on the long-time evolution of Floquet matter. **A:** Short-time evolution of $f_0$ for a drive with $\Omega = 2.6$ and $\alpha = 3$, at three different values of the s-wave scattering length $a$. Regardless of interaction strength, $f_0$ fluctuates near the PGE value (dashed line). Solid gray line shows the solution to the time-dependent Schrödinger equation for the non-interacting case. Top panel shows the driving waveform. **B:** $f_0$ as a function of time for much longer times, for the same drive and interaction parameters. Data are boxcar-averaged into 200 $\mu s$ bins. The non-interacting and weakly-interacting samples attain a second plateau (solid line) well below the PGE value (dashed line), while the strongest-interacting sample decays to a high-temperature state consistent with ergodicity. Shaded area indicates the estimated noise floor: at long times we measure no significant ground-band occupation only for the strongest-interacting sample.

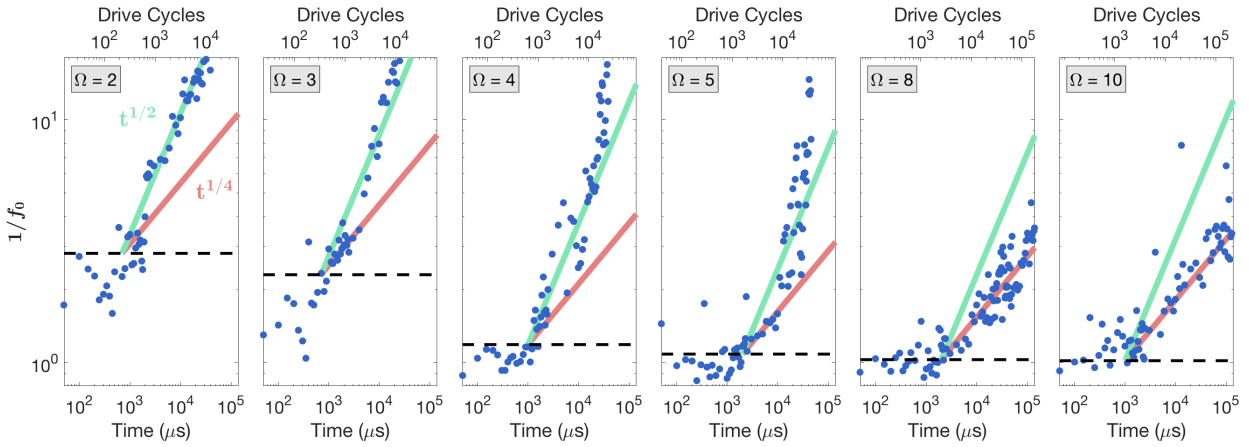


FIG. 18: Effect of drive frequency on the long-time evolution of Floquet matter. Panels show evolution of the participation ratio $1/f_0$ for $a = 30$ nm, $\alpha = 3$, and varying drive frequency $\Omega$ as indicated in the inset. Dashed line indicates the PGE prediction for the constant-$f_0$ plateau which extends as the frequency increases. The time-dependence of heating away from the prethermal plateau is observed to be strongly $\Omega$-dependent: at low frequency the participation ratio grows approximately as the square root of time (green solid line), while at the highest frequency the heating is consistent with a $t^{1/4}$ dependence (red solid line).

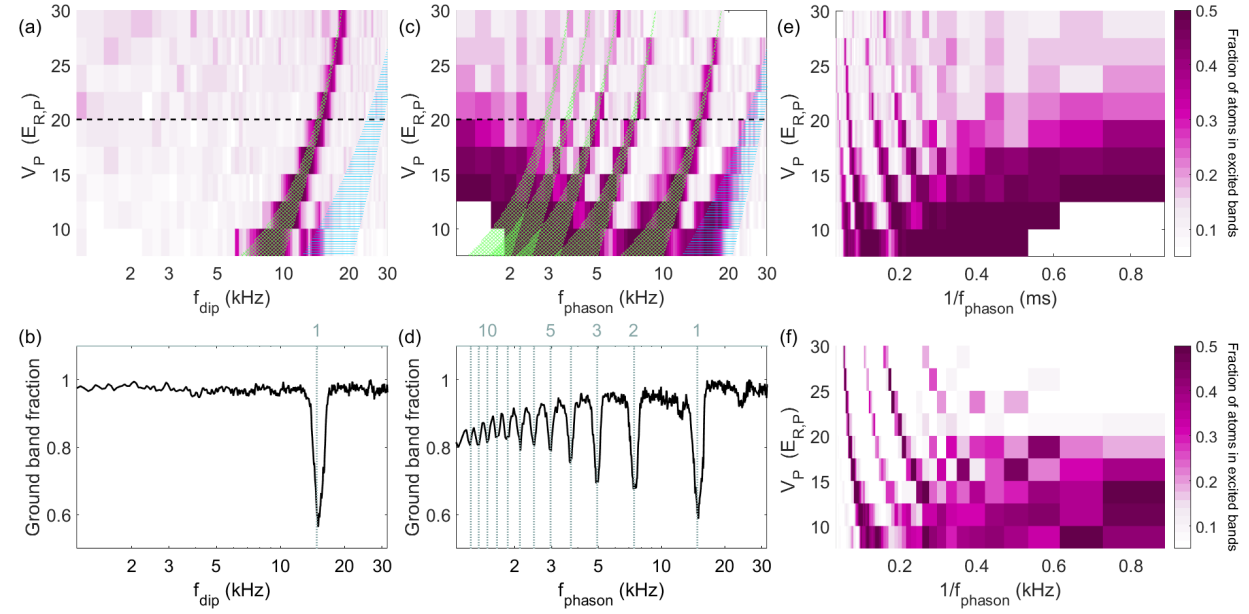


FIG. 19: Comparison of dipolar and phasonic spectroscopy. (a) Excitation due to dipolar driving as a function of drive frequency $f_{\rm dip}$ and primary lattice depth $V_P$ with $\alpha_{\rm dip} = 0.22 \times E_{R,P}/V_P$. The secondary lattice depth is fixed at $V_S = 1E_{R,S}$. Green hatched (Blue horizontally-linear) overlay shows calculated first (second) interband transition. (b) High-resolution spectrum corresponding to the line cut at $V_P = 20E_{R,P}$ in (a). Gray line shows the calculated center of the first interband transition. (c) Excitation due to phasonic driving as a function of drive frequency $f_{\rm phason}$ and primary lattice depth $V_P$. $\alpha_{\rm phason}$ is set to $\approx 1$ to match the ground band depletion of the fundamental first band transition to that of the dipolar case. Green hatched (Blue horizontally-linear) overlays show calculated first (second) interband transition, with multiphoton subharmonics also indicated for the first transition. (d) High-resolution spectrum corresponding to the line at $V_P = 20E_{R,P}$ in (c). Gray lines show the calculated center of the first twelve interband multiphoton transitions. (e) Data from (c) plotted versus drive period $1/f_{\rm phason}$, showing a broad infrared absorption feature. (f) Theoretical prediction for (e).

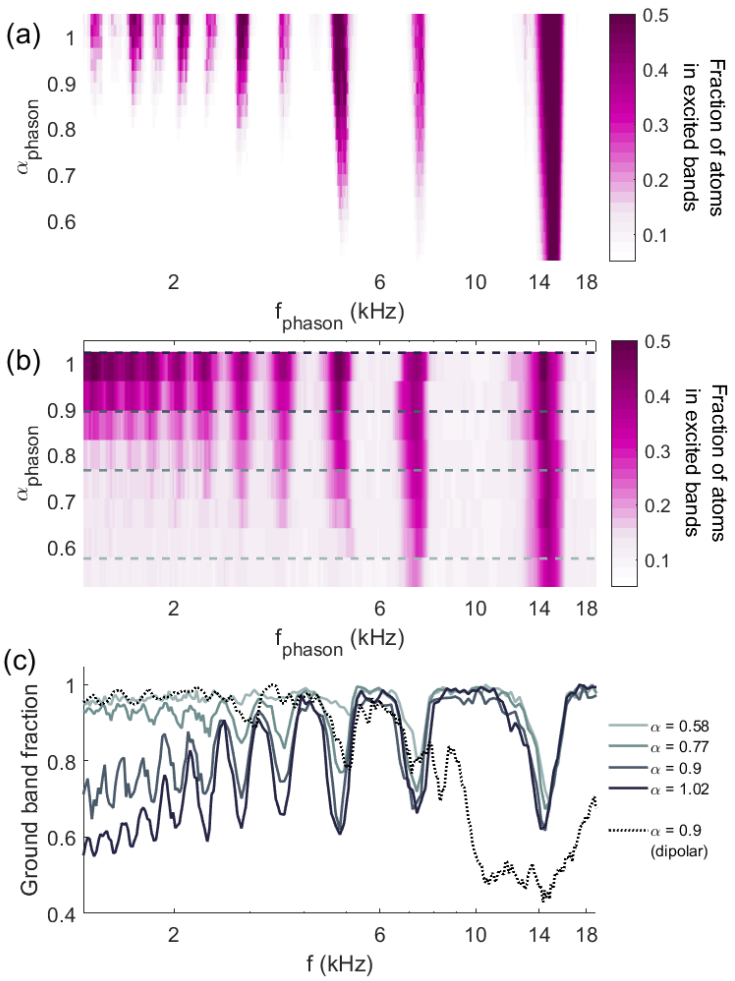


FIG. 20: Amplitude dependence of multiphoton resonances. (a) Theoretical simulation of phasonic spectra for varying drive amplitude $\alpha_{\mathrm{phason}}$. (b) Experimentally measured phasonic spectra for $V_P = 20E_{R,P}$ and varying $\alpha_{\mathrm{phason}}$. Both experiment and theory show the onset of a non-perturbative regime near $\alpha_{\mathrm{th}} = 0.9$. (c) Line cuts of experimental phasonic (solid) and dipolar (dashed) spectra at various $\alpha$ values. Note the extreme power broadening in the dipolar spectrum.

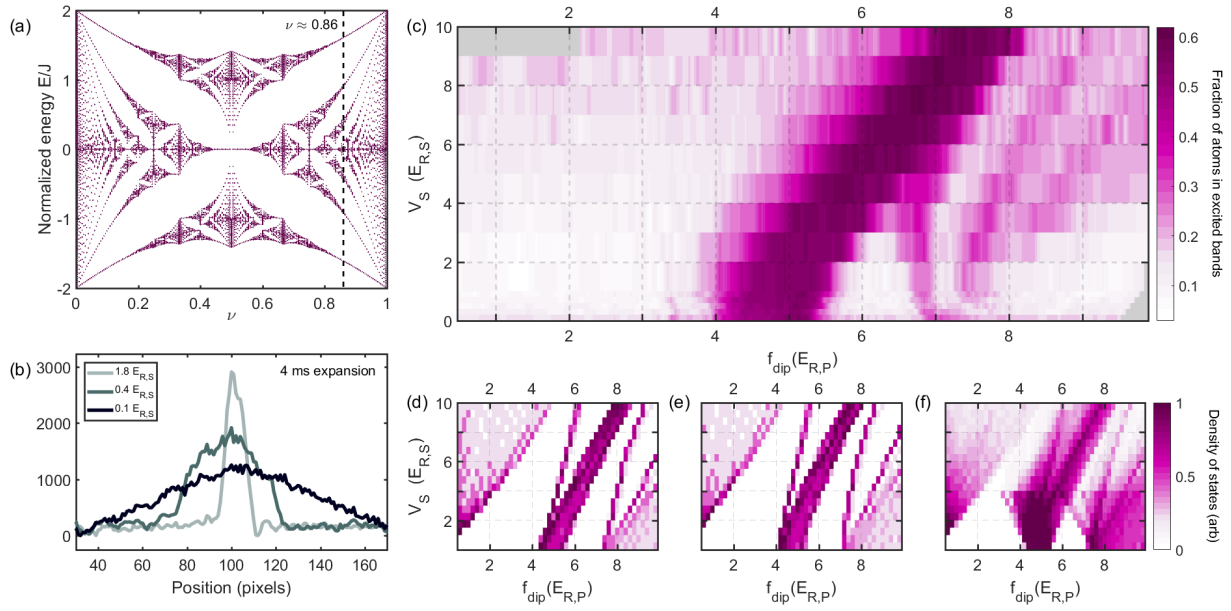


FIG. 21: Spectroscopic probing of an interacting quasicrystal. (a) Hofstadter spectrum at various lattice period ratios, $\nu = \lambda_S/\lambda_P$. Dashed line shows the slice corresponding to the quasicrystal used in this experiment. (b) Post-expansion atomic density distribution at varying disorder strengths $V_S$, showing the effects of crossing the localization transition. (c) Experimentally measured dipolar excitation spectra for varying $V_S/V_P$ at $\alpha_{\rm dip} = 0.022$, showing spectral minigaps. No data were taken for the gray areas in the upper-left and lower-right. (d) Calculated density of states for a non-interacting system, starting from a BEC. (e) Calculated density of states for an interacting BEC; a shift of the resonance line to lower frequencies is observed. (f) Calculated density of states for zero interactions, starting from a state where all single-particle orbitals below 1.5 $E_{R,S}$ are populated.

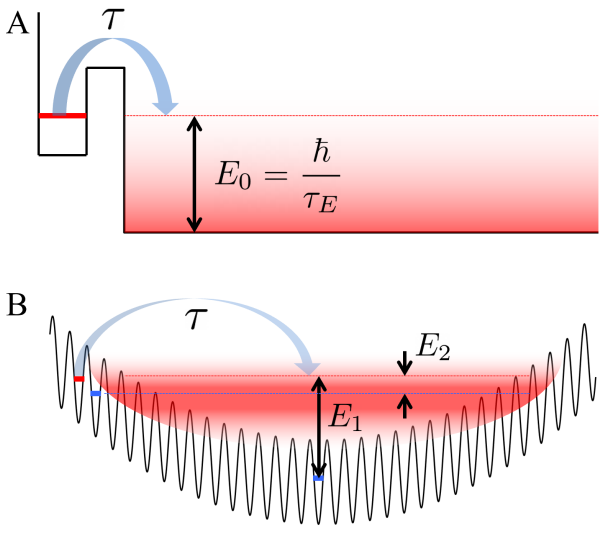


FIG. 22: A) Schematic of a potential in which non-exponential decay is expected. $\tau$ is the decay time of the exponential part of the tunneling process, and $\tau_E = \hbar/E_0$ is the timescale associated with the energy of the decay product. B) Schematic of proposed optical lattice experiment probing non-exponential decay. $E_1$ and $E_2$ are different possible characterizations of the decay product energy.

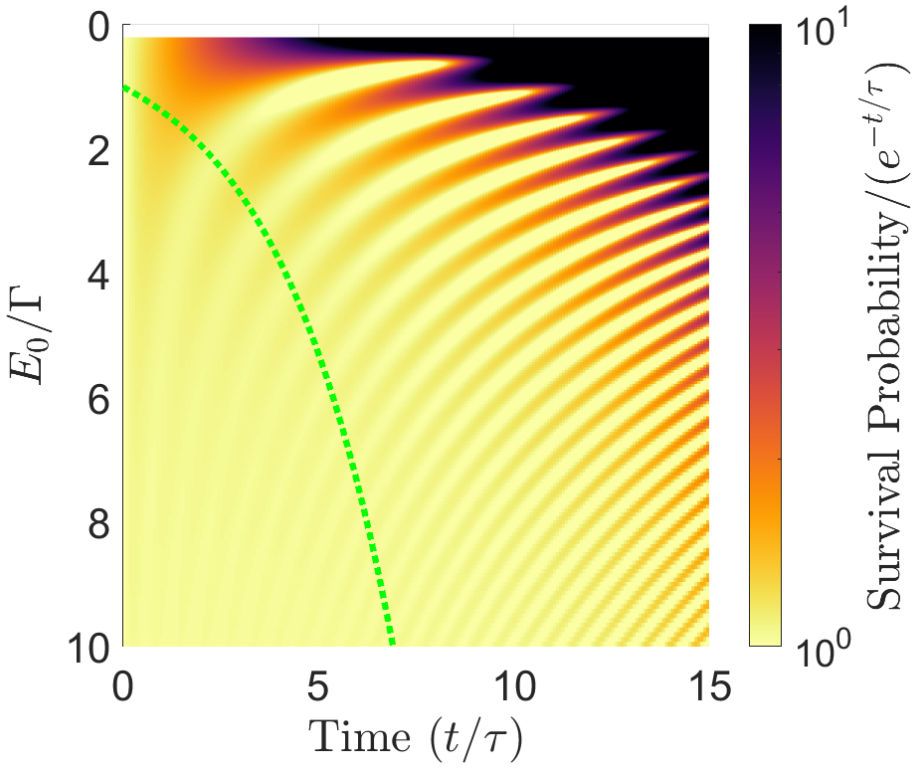


FIG. 23: Non-exponential population dynamics as a function of time and the ratio $E_0/\Gamma$. Note that the survival probability color map is normalized to an exponential law in time, with black indicating an order of magnitude population excess with respect to the exponential decay prediction. Dotted green line is the theoretical prediction for the onset of non-exponential decay.

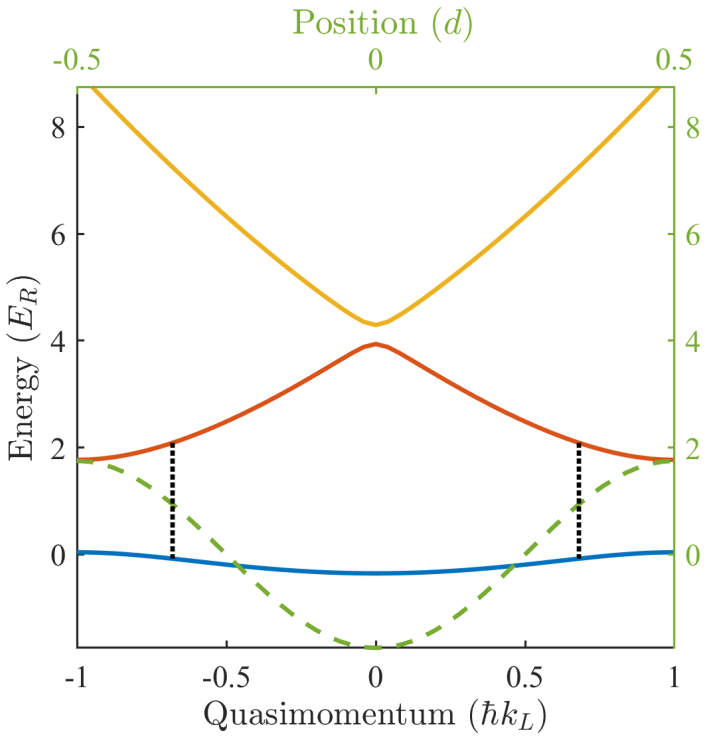


FIG. 24: Band structure of a 3.5 $E_R$ deep undriven optical lattice. Solid lines are the lowest three energy bands. Dashed line overlays the lattice potential in position space (top axis). Dotted black line depicts the drive hybridization scheme used in Figure 25, ignoring coupling to higher bands.

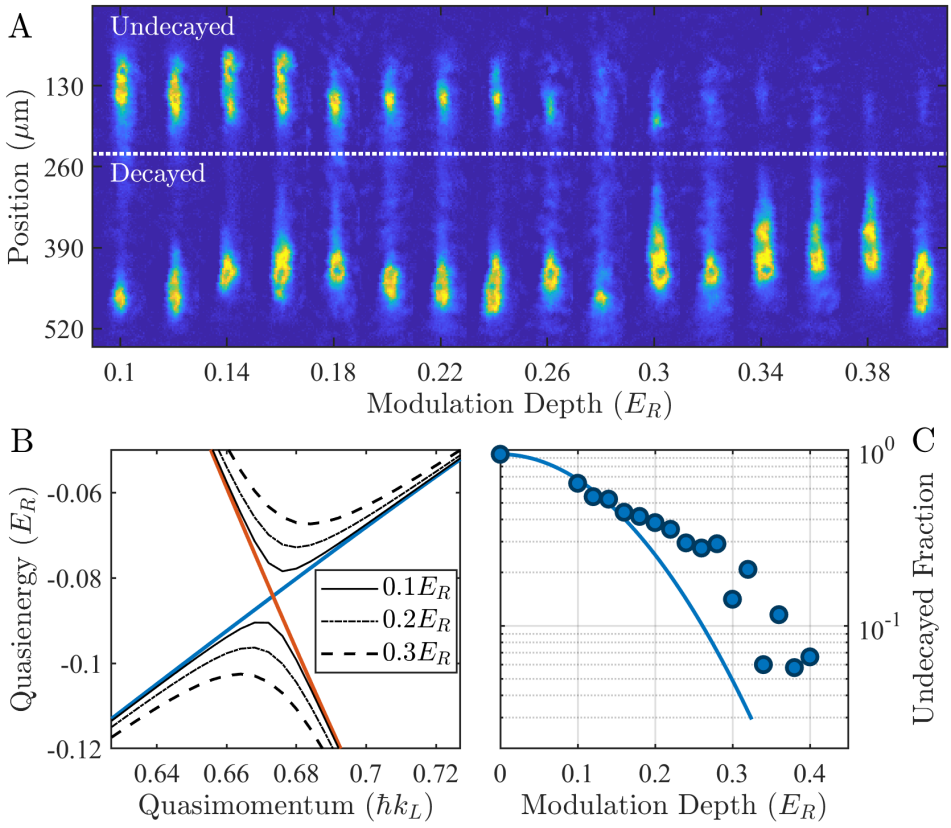


FIG. 25: Experimental demonstration of Floquet-tunable decay. A) Images of a sample of cold lithium atoms after a single Landau-Zener tunneling event during a Bloch oscillation in a quasienergy band. The "undecayed" upper cloud are those that remain in the ground band of the corresponding undriven system. The lattice depth is 3.5 $E_R$, the modulation frequency is 55 kHz, and the Bloch frequency is 27.8 Hz. B) Calculated quasienergy band structure around the avoided crossing for different modulation depths (indicated in legend). Note the drive-tunable gap. C) Undriven ground band fraction as a function of drive strength. Solid line is theory.

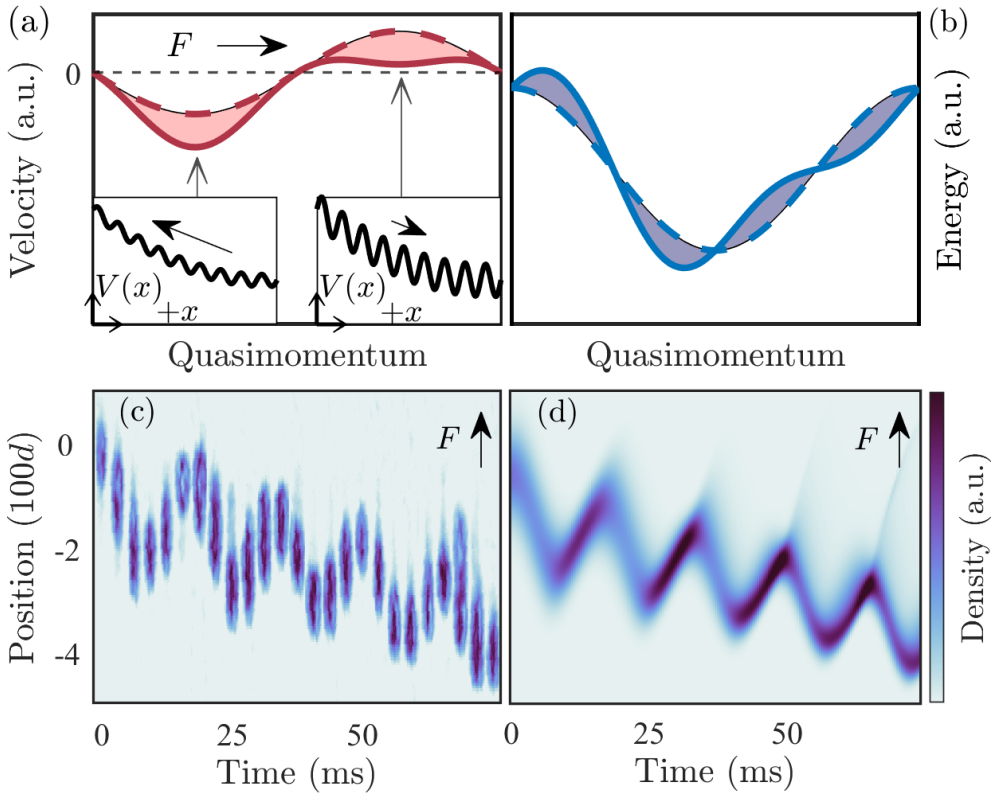


FIG. 26: Transport in a modulated lattice. (a) Comparison between convective (solid) and static (dashed) group velocity for a Bloch-oscillating ensemble with resonantly-modulated tunneling. Shaded area indicates net spatial motion over a cycle. Insets show exaggerated real-space potential, with tunneling indicated by the length and direction of the arrow. (b) Corresponding convective (solid) and static (dashed) energy bands. (c) Ordered sequence of absorption images demonstrating transport against an applied force by a chirped adaptive drive. (d) Theoretically predicted density evolution under the same conditions as (c).

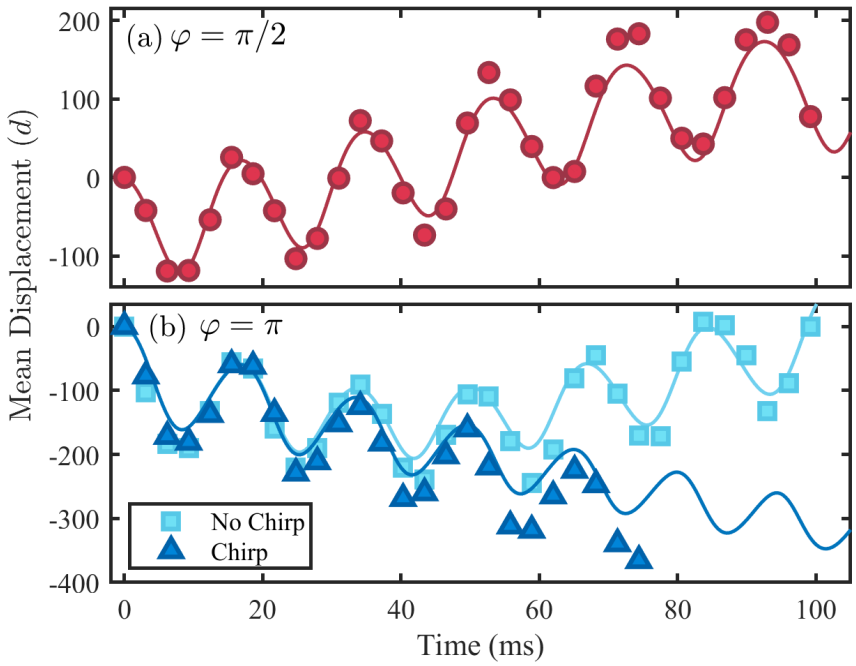


FIG. 27: Directed Floquet-Bloch transport in an inhomogeneous force field. (a) Measured (points) and numerically predicted (line) mean atomic position as a function of time for a drive phase $\varphi = \pi/2$. The applied force points towards larger positive displacements. (b) Similar measurements (points) and numerical theory (lines) for an initial drive phase $\varphi = \pi$. A time-invariant drive frequency yields epicyclic motion due to force inhomogeneity (squares). An adaptive drive using a frequency chirp suppresses this behavior and extends the range of transport (triangles, and images in Fig. 26c).

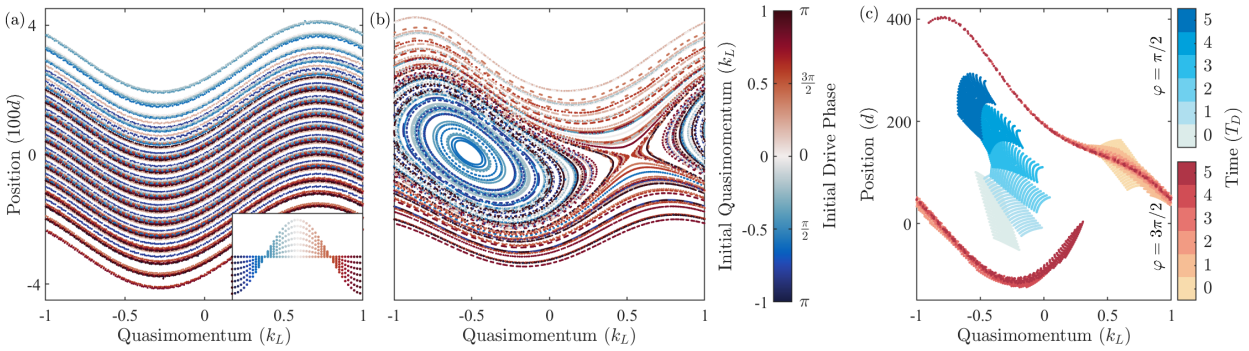


FIG. 28: Effect of the inhomogeneity-induced phase space structure on transport. (a) Stroboscopic Poincaré map for a homogeneous force at 6 Hz detuning between drive and Bloch oscillation, showing super-Bloch-like oscillations wrapping the Brillouin zone. For panels (a) and (b) an $11\times11$ grid of initial conditions spanning 400 lattice sites and the whole Brillouin zone was numerically evolved and plotted stroboscopically out to $200\,T_D$ (longer than our longest experiment times). Colorbar indicates drive phase $\varphi$, or, equivalently, initial quasimomentum. Inset shows the stroboscopic Poincaré map on identical axes out to $6\,T_D$ for zero detuning, for a single initial position over the whole quasimomentum range; trajectories unwrap yielding linear vertical transport and two invariant quasimomenta. (b) Stroboscopic Poincaré map at the same detuning, for an inhomogeneous force matching our experimental conditions. Note the emergence of nontrivial fixpoints and topologically distinct classes of orbits. (c) Short-time portrait of the evolution of an ensemble for $\varphi = \pi/2$ (blue time) and $3\pi/2$ (red time), yielding stable transport and rapid spreading respectively as a result of the different fixpoint characteristics. The plotted sample is a $21\times21$ grid spanning 1-$\sigma$ in both position and momentum.

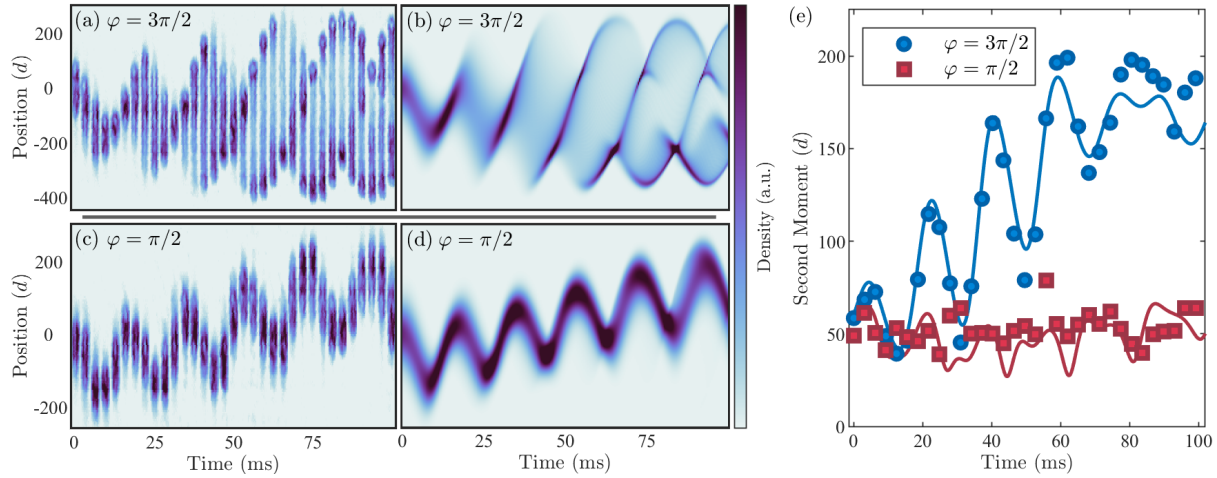


FIG. 29: Phase-dependent spatial dynamics as a probe of the stroboscopic Poincaré map. (a) and (c): Time-sequence of absorption images of an atomic ensemble subjected to drive phases of $\varphi = 3\pi/2$ (a) and $\varphi = \pi/2$ (c). These two phases are predicted to give rise to topologically distinct Poincaré orbits with qualitatively different transport dynamics, as shown in Fig. 3c. (b) and (d): Numerical simulations of the 1D density evolution under the same conditions as (a) and (c). The simulated density is averaged over independent, Gaussian-weighted 1D trials at varying lattice depths corresponding to transverse variation of beam intensity. (e) The second moment of the density distribution is plotted versus time for initial drive phases $\varphi = 3\pi/2$ (circles) and $\pi/2$ (squares). Solid lines show simulated second moment evolution, accurately capturing the asymmetric enhancement and suppression of curvature-induced monopole modes.